Basics of the LSPR Sensors for Soft Matter at Interfaces

Plasmonics
https://doi.org/10.1007/s11468-023-01812-1

Basics of the LSPR Sensors for Soft Matter at Interfaces

Vladimir P. Zhdanov[1,2]

Received: 29 January 2023 / Accepted: 23 February 2023

Abstract
An important class of localized surface plasmon resonance (LSPR)–based sensors implies the fabrication of an array of plasmonic metal nanoparticles on the support in combination with a thin protective dielectric layer. If needed, this layer can be covered, e.g., by a suitable thin biological layer, e.g., a lipid bilayer with receptors. The attachment of analyte (e.g., protein molecules or vesicles) to such interfaces is tracked via its indirect optical effect on the LSPR-related peak extinction wavelength. Such sensors have been commercialized and are now used to study biological soft matter. The length scale of the local field able in probing analyte around plasmonic nanoparticles is in this case on the order of 20 nm. Conceptually, these LSPR sensors are similar to the SPR sensors which were developed much earlier. Herein, the similarities and differences in the formalisms used to interpret SPR and LSPR measurements are discussed in detail. In particular, the exponential and power-law attenuation functions employed in these formalisms to describe the drop of the field are compared from various perspectives. The applicability of the power-law attenuation function in the context of LSPR is illustrated by using a generic model describing spherically shaped plasmonic metal nanoparticles. This model is also employed to illustrate the sensitivity of LSPR sensors with respect to various quantities. Among more specific results, the available expressions for the signal reduction factor for analyte nanoparticles of various shapes are collected and complemented by new ones. In addition, the equation describing the LSPR signal related to analyte attachment to a rough surface is presented.

Keywords LSPR and SPR sensors · Formalism · Sensitivity · Attenuation function · Reduction factor · Evanescence field

Introduction

The current rapid progress in basic nanoscience goes side by side with the efforts to use the corresponding results in applications [1, 2]. One of the best illustrations here is nanoplasmonics with its numerous applications (reviewed, e.g., in [3–5]). Among them, one of the best examples is the development of LSPR sensors for studies of various processes at interfaces (as it was first reviewed in [6]). Typically, such a sensor represents an array of ∼ 100-nm-sized plasmonic metal nanoparticles, e.g., nanodiscs (∼ 100-nm diameter and ∼ 20-nm height) fabricated (e.g., by using hole-mask colloidal lithography) on a dielectric support and covered by a thin protective dielectric film. The location of metal nanoparticles is disordered, and the average centre-to-centre distance between them is appreciable, roughly two times larger than the diameter. The LSPR measurements are usually conducted via transmission mode, whereby the spectrum of transmitted white light that passes through the sensor surface is collected for identification of the LSPR-related peak extinction wavelength, λ_{max}. Analyte is tracked by measuring the corresponding shift, $\Delta\lambda_{max}$, of λ_{max}. Basically, such sensors are formed of plasmonic nanomaterials and typically aimed at nanomaterials. Depending on the type of the interaction of analyte with plasmonic nanoparticles, the sensors under consideration can operate in the direct and indirect regimes [6].

In the direct regime, the analyte penetrates into plasmonic metal nanoparticles and literally interacts with them. The best example is perhaps tracking of the presence of hydrogen in air [7]. In the corresponding sensors, the protective layer lets hydrogen through, and it is reversibly absorbed by plasmonic nanoparticles, so that the sensor output, $\Delta\lambda_{max}$, is determined by the hydrogen uptake. From the perspective of hydrogen absorption, the most suitable plasmonic

✉ Vladimir P. Zhdanov
zhdanov@chalmers.se; zhdanov@catalysis.ru

[1] Section of Nano and Biophysics, Department of Physics, Chalmers University of Technology, S-41296 Gothenburg, Sweden

[2] Boreskov Institute of Catalysis, Russian Academy of Sciences, 630090 Novosibirsk, Russia

Published online: 27 March 2023

metal is Pd. At room temperature, it easily absorbs appreciable amount of hydrogen in the stepwise fashion due to the first-order phase transition. The latter is inconvenient in the context of sensing. To make the response gradual, Pd is alloyed with another metal, e.g., Au ($\sim 5-8\%$; see experiments [7] and DFT-based analysis of the corresponding absorption isotherms [8]). Such sensors are now superior in the context of detection limit and response time but have not been commercialized yet.

In the indirect regime, the analyte is deposited on the protective layer or on a thin layer covering the protective layer and does not directly contact plasmonic metal nanoparticles. The light-induced electric field acting on analyte is composed of the intrinsic electric field of light and the field related to polarization of a plasmonic nanoparticle. Due to the difference of the analyte dielectric permeability and that of the surrounding medium (e.g., water), analyte influences the electric field inside plasmonic nanoparticles, and this feedback results in the observed signal, $\Delta\lambda_{\max}$. The LSPR sensors of this type were commercialized (e.g., by Insplorion AB, Gothenburg, Sweden) and are now in the use especially in studies of biologically relevant soft matter as reviewed in [9, 10] (among complementary reviews, I can mention, e.g., [11–14]). The focus is often on the changes in the shape of adsorbed biomolecules [15–17] and biological nanoparticles, such as lipid vesicles under various conditions [18]–[27]. Remodeling of a supported lipid bilayer with the formation of buds and tubules has been explored as well [28].

As usual for scientific instruments, the development, function, and interpretation of the output of the LSPR sensors are based on the general physical concepts and corresponding formalism. From this perspective, the theoretical basis underlying such sensors can be improved. Following this line, I focus herein on the indirect LSPR sensors. Conceptually, the physics behind such sensors is qualitatively similar to that behind the SPR sensors employing a thin plasmonic metal film (typically Au). The latter sensors and corresponding formalism were developed long ago (reviewed in [29–31]). With some reservations, this formalism was literally used in the first applications of the LSPR sensors (reviewed in [32]). Despite subsequent modifications (briefly reviewed in [27]), the LSPR formalism is still incomplete and has not been systematically described in the available reviews (e.g., [9]–[14]) and original studies. My goal is to fill this gap at least partially.

The main presentation below (in the section entitled "Results and Discussion") is focused on three general issues. First, extending the introduction, I outline the basics of the SPR sensors (in the first and second subsections) and the corresponding LSPR modifications (in the third subsection). In addition to the results already available in the literature (see, e.g., [27]), this part contains some novel elements from the SPR and LSPR perspectives including (i) illustration of the similarity and difference of two attenuation functions for the field and the corresponding reduction factors used to interpret the SPR and LSPR signals, (ii) explicit expressions of the reduction factor for some specific shapes of analyte, and (iii) equation for describing the SPR or LSPR response to attachment of analyte to a rough surface. Second, I use a generic exactly solvable toy model in order to illustrate the physics behind the LSPR sensors (in the fourth subsection). Third, I discuss the sensitivity of the LSPR sensors with respect to the analyte dielectric permeability and thickness (in the fifth subsection). A brief outcome of the analysis is given afterwards (in the section entitled "Conclusions").

Regarding the presentation, I can add two remarks. First, I discuss various aspects of the SPR and LSPR formalisms and use various models. Under such conditions, the full-scale detailed introduction is impossible. In particular, the introduction above contains primary references for general orientation. More specifical introductory references are given below. Second, my article is aimed at general readership, including primarily the experimentalists using the indirect LSPR sensors. To make the presentation suitable for such readers, I use partly colloquial and informal style and partly textbook style where it is needed.

Results and Discussion

General Equations for SPR

In conventional SPR sensors, the output is induced by the interaction of analyte with the evanescent field,

$$E = E_{\circ}\exp(ikx - z/2\delta), \tag{1}$$

where $E_{\circ}$ is the amplitude at the interface, k is the wave propagation constant, δ is the penetration depth determined by the Fresnel equations, and x and z are the coordinates along and perpendicular to the interface, respectively. In measurements, the output, R, is identified with the shift in either SPR wavelength or observation angle. If the analyte film is thin ($\ll \delta$), the field extinction becomes irrelevant, and R is proportional to a product of the analyte mass or average thickness, $\langle d\rangle$, and the difference of the analyte and solution refractive indexes, $\Delta n \equiv n_{\mathrm{a}} - n_{\mathrm{s}}$. If the extinction is not negligible, the response is modulated by the corresponding attenuation function, $\exp(-z/\delta)$, and can be rather accurately represented as [33]

$$R = S\int_0^{\infty} \Delta n(z)\exp(-z/\delta)\mathrm{d}z/\delta, \tag{2}$$

where S is the sensitivity factor, and $\Delta n(z)$ is the z-dependent factor averaged along the x and y directions. This expression is fairly general and applicable to uniform films as well as to heterogeneous systems with spatial distribution of attached

particles of different shape and composition. One of the conditions of its applicability is that Δn is relatively small so that the value of δ is close to that in solution in the absence of analyte.

For a uniform film of thickness d, Eq. (2) yields

$$R = S\Delta n[1 - \exp(-d/\delta)], \quad \text{or} \quad R = S\Delta n d\delta^{-1}\varphi, \tag{3}$$

where

$$\varphi = [1 - \exp(-d/\delta)]\delta/d \tag{4}$$

is a dimensionless factor (≤ 1) taking the evanescent-field-related reduction of R into account.

For attached nanoparticles of one type, Eq. (2) can be rewritten as (see Eq. (6) in combination with (4) in [34])

$$R = S\Delta n c v_{\mathrm{m}}\delta^{-1}\varphi, \quad \text{with} \quad \varphi = \int_0^{z_*} \frac{\mathrm{d}v(z)}{\mathrm{d}z}\exp(-z/\delta)\mathrm{d}z/v_{\mathrm{m}}, \tag{5}$$

where c is the surface concentration of nanoparticles, v_* is the integral volume of molecules forming a nanoparticle (if a nanoparticle has no hollows, this is its volume), $v(z)$ is the integral volume of molecules in a nanoparticle in the region from 0 to z, and z_* is the maximum value of z in a nanoparticle (according to the latter two definitions, $v(z_*) \equiv v_{\mathrm{m}}$).

Regarding the transition from (2) to (5), one should bear in mind that (2) is directly applicable to films which are homogeneous along the x and y directions, whereas (5) is proposed for systems which are heterogeneous along these directions. In general, the scattering of light in heterogeneous systems is described by cumbersome equations. Although the corresponding theoretical studies have long history, the compact results relevant in the context of SPR or LSPR sensors are lacking. The use of (2) or (5) for such systems is possible provided one can operate by the effective refractive index which is independent of x and y. The corresponding necessary condition appears to be that $2\pi/k$ (k is defined by (1)) is larger than or at least comparable with the size of analyte nanoparticles and the distance between them.

Some analyte nanoparticles of complex composition can be characterized by spatially dependent refractive index. In lipid nanoparticles containing mRNA, for example, the latter can be located closer to the center, and it results in the spatially dependent refractive index, because the lipid and mRNA refractive indexes are different. In such cases, Eq. (5) can be modified as

$$R = Sc\delta^{-1}\int_0^{z_*} \Delta n(z)\frac{\mathrm{d}v(z)}{\mathrm{d}z}\exp(-z/\delta)\mathrm{d}z, \tag{6}$$

where $\Delta n(z)$ is the refractive-index difference averaged over x and y.

The SPR technique can also be used to explore deposition of biomolecules or nanoparticles on a rough substrate fabricated on the surface of a sensor (by analogy with the studies performed by employing quartz crystal microbalance with dissipation and ellipsometry [35]). In this case, the substrate-solution interface profile can be described by height, $h(x, y)$, or, more specifically, the h distribution, $F_{\mathrm{s}}(h)$, whereas the adsorbate can be characterized by thickness, $d(x, y)$, or the d distribution, $F_{\mathrm{a}}(d, h)$, calculated at each h. Then, according to (2) and (3), the adsorbate-related contribution to the SPR signal can be represented as

$$R = S\Delta n\int_0^{\infty}\int_0^{\infty} \exp(-h/\delta)[1 - \exp(-d/\delta)]F_{\mathrm{a}}(d, h)F_{\mathrm{s}}(h)\mathrm{d}d\mathrm{d}h. \tag{7}$$

For thin substrate and adsorbate films ($\ll \delta$), as expected, this expression yields $R = S\Delta n\langle d\rangle/\delta$. In general, however, the calculation of the response is far from straightforward because one should first specify $F_{\mathrm{s}}(h)$ and $F_{\mathrm{a}}(d, h)$.

Reduction Factors for Specific Systems

For a uniform film or objects with well-defined thickness, d, in the direction perpendicular to the interface (e.g., analyte islands or disk-like nanoparticles), the evanescent-field-related reduction factor, φ, is given by (4). For analyte nanoparticles of other specific shapes, φ is determined by (5) and can be calculated analytically or numerically. The corresponding results are applicable not only to SPR and LSPR but also in the context of total internal reflection fluorescence microscopy (TIRFM; see, e.g., [36]).

For a thin spherical shell of arbitrary size, the expression φ is identical to that for a uniform film despite the apparent difference of the mass distribution [34, 36], i.e., one can use Eq. (4) and identify d there with the shell diameter (i.e., $d = 2r$, where r is the shell radius). This model is of interest in the context of vesicles linked to the substrate by a few bonds so that their shape remains spherical. Deformed attached vesicles can be viewed as a truncated thin spherical shell with a flat basement. For the latter model, Eq. (4) can easily be adapted as well [27, 34].

For fully filled spherically shaped nanoparticles of size $2r$, the reduction factor is given by Eqs. (10)–(12) in [27] and can be represented in a more compact form (compared to [27]) as

$$\varphi_{\mathrm{s}} = 3\left(\frac{\delta}{r}\right)^3 \exp\left(-\frac{r}{\delta}\right)\left[\frac{r}{\delta}\cosh\left(\frac{r}{\delta}\right) - \sinh\left(\frac{r}{\delta}\right)\right]. \tag{8}$$

Its dependence on r/δ is explicitly shown in Fig. 1(a).

For a spherical shell of finite thickness, φ can be calculated by using (8) for a whole sphere and then subtracting a similar expression for a core,

$$\varphi = \frac{r_{\mathrm{s}}^3}{r_{\mathrm{s}}^3 - r_{\mathrm{c}}^3}\left[\varphi_{\mathrm{s}}(r_s) - \frac{r_{\mathrm{c}}^3\varphi_{\mathrm{s}}(r_c)}{r_{\mathrm{s}}^3}\exp\left(-\frac{r_{\mathrm{s}} - r_{\mathrm{c}}}{\delta}\right)\right], \tag{9}$$

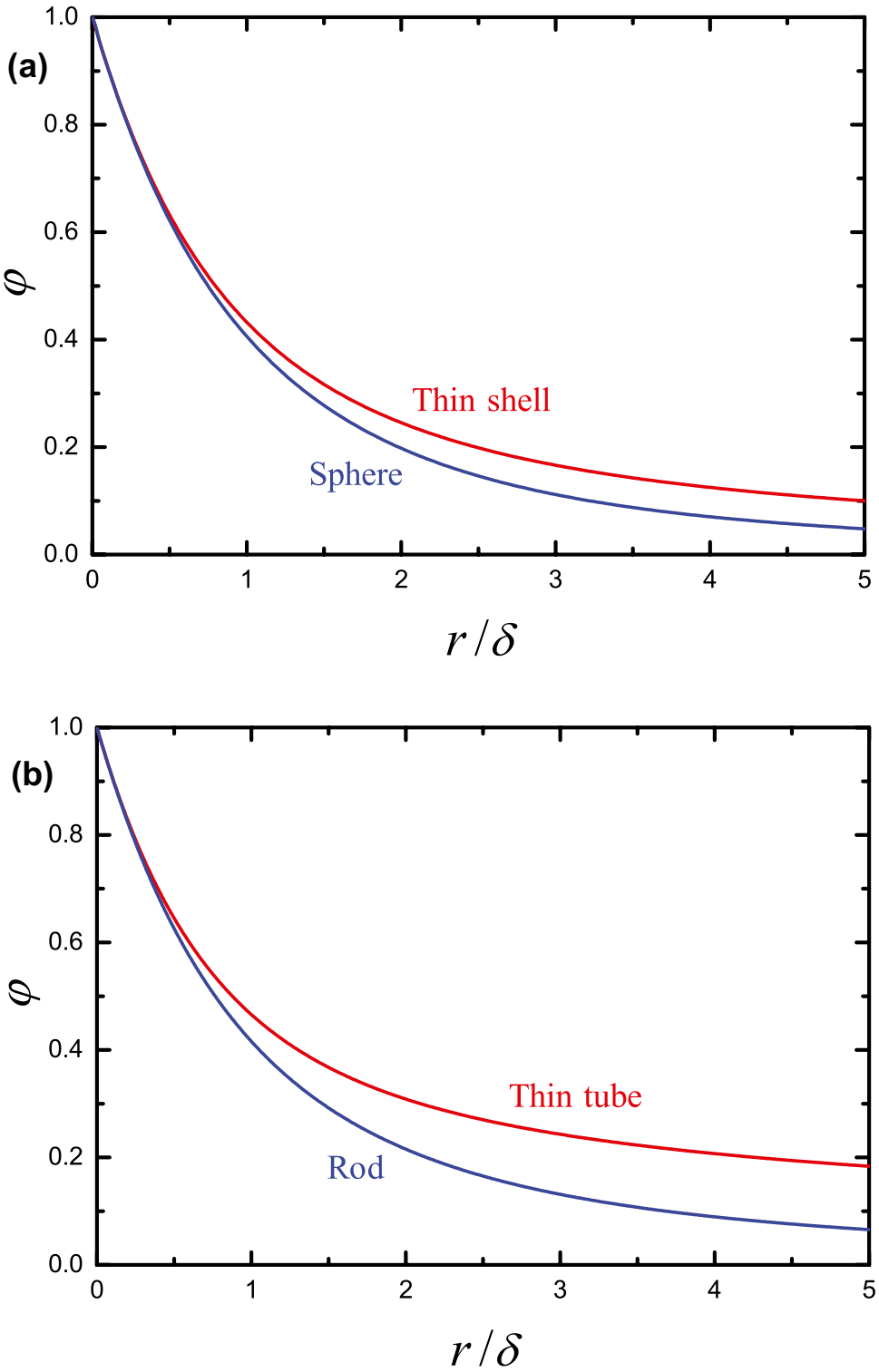

Fig. 1 Reduction factor as a function of r/δ: **a** thin spherical shells (Eq. (4)) and fully filled spheres (Eq. (8)), and **b** thin cylindrical tubes (Eq. (10)) and fully filled cylinders (Eq. (11)). The factors for fully filled objects are somewhat smaller because the mass is located primarily in the central region and its contribution to the signal is reduced

where r_s and r_c are the external and internal radii. If $r_c \to r_s$, one can prove that this expression becomes to be identical to (4) provided d is identified there with $2r_s$. The difference between (4) and (9) in the case of vesicles of ~ 100-nm size is shown in Fig. 2.

For nanoparticles with the cylindrical symmetry, including thin nanotubes, nano-rods (e.g., elongated viruses such as rhabdovirus), and nanotubes of finite thickness (e.g., lipid tubules), φ is given by (4) in the case of orientation perpendicular to the interface as it has already been noticed

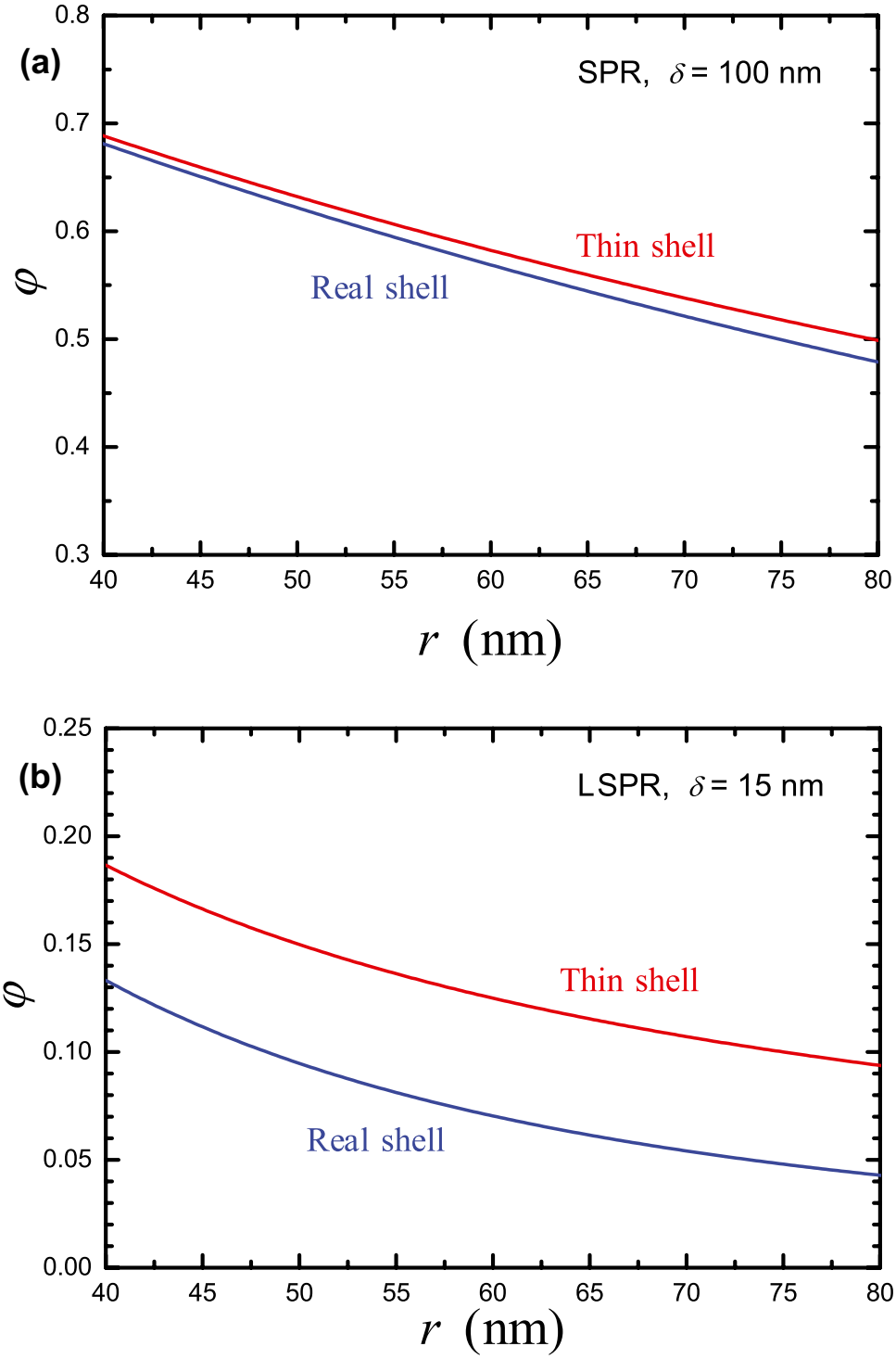

Fig. 2 Reduction factor for spherical lipid vesicles as a function of radius (from 40 to 80 nm) in the cases when the lipid-bilayer thickness is neglected (Eq. (4) with $d = 2r$] and taken into account (Eq. (9) with $r_s - r_c = 4.5$ nm). **a** and **b** show the results for $\delta = 100$ nm (typical for SPR sensors) and 15 nm (typical for LSPR sensors), respectively. The thickness is negligible in the former case and not negligible in the latter case

in the beginning of this section (d should here be identified with the nanoparticle length). If nanoparticles of these types lie at the interface, φ is represented, respectively, as

$$\varphi = \frac{1}{\pi}\int_0^{\pi} \exp[-r(1+\cos\phi)/\delta]\mathrm{d}\phi, \tag{10}$$

$$\varphi_\mathrm{r} = \frac{2}{\pi}\int_0^{\pi} \exp[-r(1+\cos\phi)/\delta]\sin^2\phi\,\mathrm{d}\phi, \tag{11}$$

$$\varphi = \frac{r_\mathrm{r}^2}{r_\mathrm{r}^2 - r_\mathrm{c}^2}\left[\varphi_\mathrm{r}(r_r) - \frac{r_\mathrm{c}^2\varphi_\mathrm{r}(r_c)}{r_\mathrm{r}^2}\exp\left(-\frac{r_\mathrm{r}-r_\mathrm{c}}{\delta}\right)\right], \tag{12}$$

where r_r and r_c are the external and internal radii. The corresponding integrals (in (10) and (11)) are not expressed via elementary functions but can easily be calculated numerically (Fig. 1(b)).

Analytical expressions for φ can be obtained in some other cases, e.g., for pyramidally or conically shaped nanoparticles contacting the interface by their base.

General Remarks Regarding LSPR

As already noticed in the "Introduction," the SPR formalism outlined in the previous two subsections (especially the simplest version given by Eqs. (3) and (4)) was used literally in the first applications of the LSPR sensors [32] and is still employed now (see, e.g., [27], references therein, and Supplementary Information in [28]). In this framework, all the expressions for the SPR reduction factors for specific systems (in the subsection above) can be employed in the LSPR case as well. Concerning the corresponding reservations, one can notice that in SPR the decay of the evanescent field is exponential and the corresponding decay length, δ, is defined by the light frequency and optical constants of the media; whereas in LSPR, the evanescent field around sensing metal nanoparticles contains different terms (dipole etc.), and the corresponding decay length is roughly proportional to and significantly smaller than the average nanoparticle size. For this reason, the exponential attenuation function, $\exp(-z/\delta)$, used validly in the SPR formalism should be viewed just as a fitting function if this formalism is employed in the LSPR case. For uniform analyte films and sensing plasmonic nanodiscs of 20-nm height and diameter ranging from 80 to 160 nm, the applicability of this function was demonstrated, e.g., by electrodynamic simulations based on the finite-difference time-domain (FDTD) method [27]. With increasing diameter, δ was found to increase from 10 to 20 nm.

Taking into account that the dipole interaction dominates in LSPR, the exponential attenuation function was proposed to be replaced by the dipole one, $\propto 1/(R_* + z)^6$, where R_* is the length scale (effective radius) characterizing plasmonic nanodiscs [18]. The latter attenuation function can be used literally as $1/(R_* + z)^6$ [18], or by analogy with the exponential attenuation function it can be normalized so that its value is equal to unity at $z = 0$, i.e., as $R_*^6/(R_* + z)^6$ [28]. This function appreciably drops at $z \simeq R_*/5$, and this value can be compared to δ in the exponential attenuation function. For sensing nanodiscs of 20 nm height and diameter ranging from 70 to 210 nm, the effective radius is roughly in the range from 35 to 100 nm, and the scale characterizing the drop of the dipole function is expected to be from 8 to 20 nm. This is in agreement with the results of the FDTD calculations mentioned above and slightly smaller than in the experiments with sensing nanodiscs of 20 nm height and 74 and 210 nm diameter [27]. In addition, the dipole approximation indicates that the drop of the exponential attenuation function is independent of the solution refractive index and explains why this is the case. This is in agreement with the results of the abovementioned FDTD calculations as well. For additional FDTD calculations, one can see ref. [20].

In the context of LSPR with the dipole attenuation function, Eq. (9) can be rewritten as

$$\Delta\lambda_{\max} = S\int_0^\infty \Delta n(z)\frac{5R_*^5}{(R_* + z)^6}\mathrm{d}z. \tag{13}$$

For a uniform film, this expression yields

$$\Delta\lambda_{\max} = S\Delta n\left(1 - \frac{R_*^5}{(R_* + d)^5}\right), \quad \text{or} \quad \Delta\lambda_{\max} = S\Delta n\left(\frac{5d}{R_*}\right)\varphi, \tag{14}$$

where

$$\varphi = \frac{R_*}{5d}\left(1 - \frac{R_*^5}{(R_* + d)^5}\right) \tag{15}$$

is the reduction factor (≤ 1) defined by analogy with (4).

The use of Eqs. (13)–(15) implies that $\Delta\lambda_{\max}$ is dominated by the local effect of analyte on each plasmonic nanodisc. The multiple scattering of light by nanodiscs is not treated explicitly. For the LSPR sensors under consideration (with appreciable average distance between nearly randomly located nanodiscs), the contribution of multiple scattering to $\Delta\lambda_{\max}$ is typically small (about 10 nm; see, e.g., the calculations in [37]) and can be included into the LSPR measurement baseline, the contribution of analyte is small as well (also about 10 nm), and both factors can be considered as perturbations. The mutual influence of these factors is a second-order correction and can be neglected. In fact, Eqs. (13)–(15) are expected to be applicable also for regularly located nanodiscs (the multiple scattering can be included into S and the measurement baseline). For other types of LSPR sensors, e.g., those focused on analyte located in the narrow contact region in a pair of adjacent plasmonic nanoparticles which are very close together (reviewed, e.g., in [13]; for the related calculations, see, e.g., [38, 39] and references therein), the formalism should obviously be different. Although the latter case is of interest from various perspectives, its analysis is beyond my goals.

To compare the exponential and dipole attenuation functions and the related expressions (4) and (15) for φ, it is useful to introduce the distance, $z_{0.5}$, corresponding to the drop of an attenuation function by 50%. For the functions under consideration, these distances are given by $\ln(2)\delta$ (or 0.693δ) and $(2^{1/6} - 1)R_*$ (or $0.123R_*$). Then, the comparison can be done by using $z_{0.5}$ for normalization of the abscissae (Fig. 2). This normalization helps to compare the shape of the normalization

functions despite their dependence on different parameters. The agreement between the exponential and dipole attenuation functions is seen to be good provided z is not large (Fig. 3(a)). If z is large, the dipole attenuation function is larger than the exponential one. The agreement between the exponential and dipole reduction factors is fairly good as well (Fig. 3(b)). With increasing d, the dipole reduction factor is also somewhat larger than the exponential one, but the difference is smaller than that for the attenuation functions.

The conventional SPR or LSPR sensors imply one-band measurements. In the LSPR case, this means the use of sensing metal nanodisks of one type. The dual-band modes of

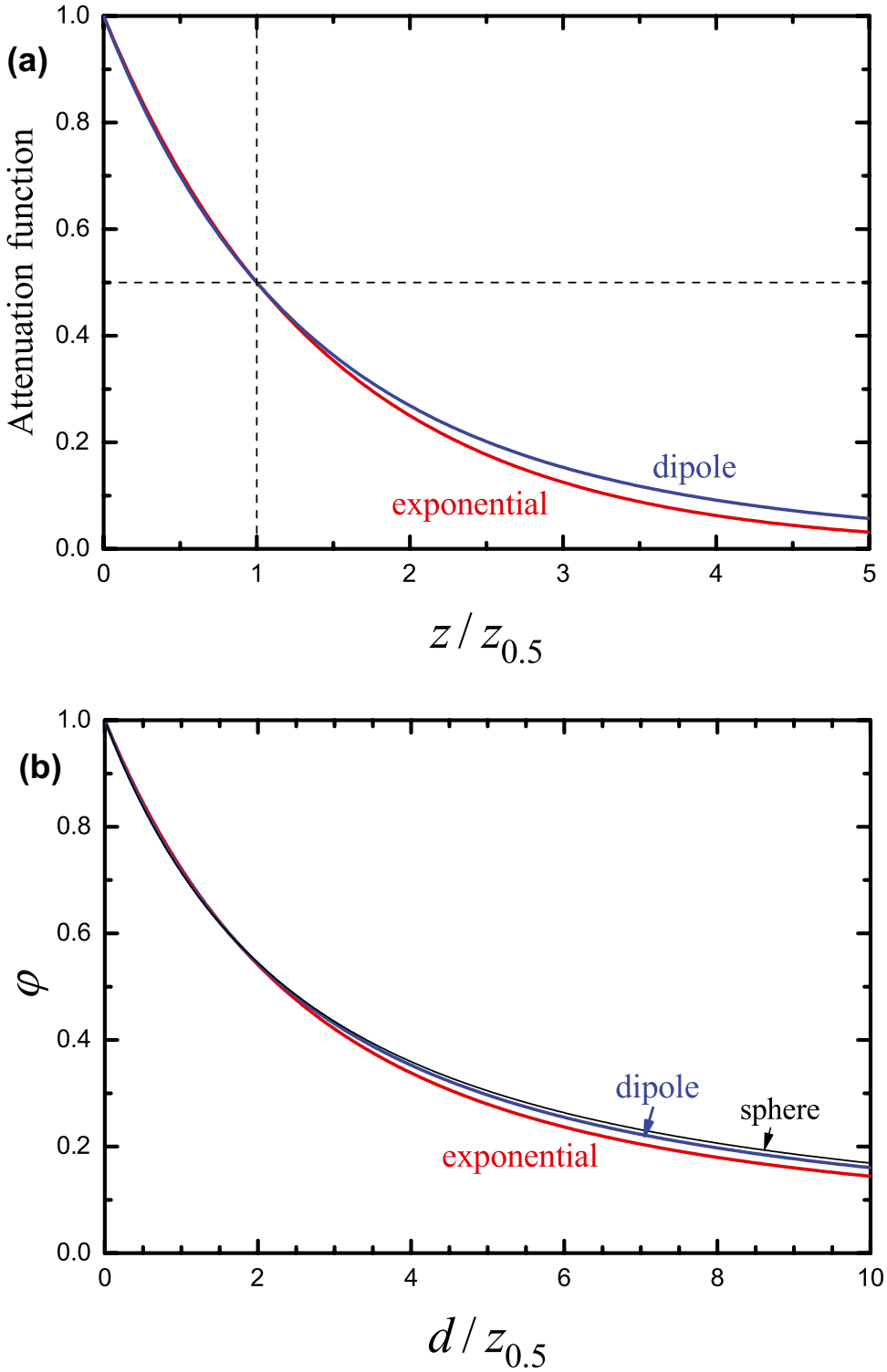

Fig. 3 **a** Exponential and dipole attenuation functions and **b** related reduction factors ((4) and (15)) for a uniform layer as a function of normalized coordinate and layer thickness, respectively. The factor marked by "sphere" corresponds to (32)

SPR or LSPR measurements are also possible and allow one to obtain more information about analyte [27, 34]. The formalism presented above is applicable for both modes of SPR or LSPR measurements.

Generic Model of the LSPR Sensors

The results presented in the three subsections above are oriented to applications of SPR and LSPR sensors. In the context of physics, it is of interest to use an exactly solvable toy model in order to clarify the applicability of the dipole approximation and the way how the refractive indexes or dielectric permittivities can be taken into account. Following this line, I scrutinize here the LSPR response, related to deposition of an analyte film on a single spherical plasmonic metal nanoparticle. For the LSPR sensors under consideration, the analysis of this simplest situation is relevant because, as explained in the paragraph below Eq. (15), the effect of the interaction of nanoparticles can be viewed as perturbation and included into the LSPR measurement baseline.

Now, as already noticed in the subsection above, the LSPR sensors usually include metal nanodiscs. Such nanodiscs can be approximated by an ellipsoid or, in other words, "spheroid" [40]. The specifics of the interaction of spheres and ellipsoids with light are similar [41]. The equations for an ellipsoid are, however, cumbersome. From the latter perspective, the focus on a sphere is preferable. In physics, the optical response of nanoparticles is customarily described in terms of dielectric permittivities and light frequency, ω. This is a reason why I use in this subsection the analyte-related frequency shift, $\Delta\omega_{\mathrm{LSPR}}$, and dielectric permittivities, despite the traditional use of $\Delta\lambda_{\mathrm{max}}$ and refractive indexes in the articles related to LSPR sensors (e.g., in the subsection above).

A spherically shaped metal nanoparticle of radius R is considered to be covered by a uniform film of thickness d. Basically, this is a conventional core-shell model. In the context of plasmons, it can be analyzed analytically in terms of phenomenological dielectric permittivities [41] or numerically from first principles [42]. I employ the former approach. Earlier, it was already used in the related literature (see, e.g., [43, 44]) but not from the perspective of the LSPR sensors.

In the Rayleigh limit, the intensity of light scattering by a metal nanoparticle covered by film can be represented as

$$I = A|\alpha|^2, \tag{16}$$

where α is the nanoparticle+film polarizability calculated in the static approximation, and A is a constant (this constant includes the squared tensity of the electric field of incident light). For a spherical nanoparticle in solution alone, the polarizability is well known to be given by [41]

$$\alpha = 4\pi r^3 \frac{\epsilon_{\mathrm{m}} - \epsilon_{\mathrm{s}}}{\epsilon_{\mathrm{m}} + 2\epsilon_{\mathrm{s}}}, \tag{17}$$

where ϵ_{m} and ϵ_{s} are the metal and solution permittivities. For a spherical nanoparticle covered by a film, the polarizability can be represented as (see, e.g., Eq. (5.36) in [41])

$$\alpha = 4\pi(R+d)^3 \frac{(\epsilon_{\mathrm{f}} - \epsilon_{\mathrm{s}})(\epsilon_{\mathrm{m}} + 2\epsilon_{\mathrm{f}}) + f(\epsilon_{\mathrm{m}} - \epsilon_{\mathrm{f}})(\epsilon_{\mathrm{s}} + 2\epsilon_{\mathrm{f}})}{(\epsilon_{\mathrm{f}} + 2\epsilon_{\mathrm{s}})(\epsilon_{\mathrm{m}} + 2\epsilon_{\mathrm{f}}) + 2f(\epsilon_{\mathrm{m}} - \epsilon_{\mathrm{f}})(\epsilon_{\mathrm{f}} - \epsilon_{\mathrm{s}})}, \tag{18}$$

where ϵ_{f} is the film permittivity, and

$$f = R^3/(R+d)^3 \tag{19}$$

is the fraction of the metal+film volume occupied by the metal.

In the absence and presence of analyte, the LSPR frequency, ω_{LSPR}, is determined, respectively, by the pole of (17) or (18), i.e., by the following conditions

$$\mathrm{Re}\,(\epsilon_{\mathrm{m}} + 2\epsilon_{\mathrm{s}}) = 0, \quad \text{or} \tag{20}$$

$$\mathrm{Re}\,[(\epsilon_{\mathrm{f}} + 2\epsilon_{\mathrm{s}})(\epsilon_{\mathrm{m}} + 2\epsilon_{\mathrm{f}}) + 2f(\epsilon_{\mathrm{m}} - \epsilon_{\mathrm{f}})(\epsilon_{\mathrm{f}} - \epsilon_{\mathrm{s}})] = 0. \tag{21}$$

In the latter equation, it is convenient to add unity to and subtract it from f and then to keep separately the term proportional to $1-f$. This yields

$$\mathrm{Re}\,[3\epsilon_{\mathrm{f}}(\epsilon_{\mathrm{m}} + 2\epsilon_{\mathrm{s}}) - 2(1-f)(\epsilon_{\mathrm{m}} - \epsilon_{\mathrm{f}})(\epsilon_{\mathrm{f}} - \epsilon_{\mathrm{s}})] = 0. \tag{22}$$

This form of Eq. (21) is preferable, because the second term vanishes in the absence of analyte (at $f = 1$), and in this limit one gets Eq. (20). In the presence of analyte, the second term inducing $\Delta\omega_{\mathrm{LSPR}}$ can be considered as a perturbation because its value is small.

Using (22) in the context of LSPR sensors, one should take into account that ϵ_{m} contains real and imaginary parts and is strongly dependent on ω, whereas ϵ_{s} and ϵ_{f} can be considered to be real and independent of ω. In addition, ϵ_{f} is typically close to ϵ_{s}. The latter means that $(\epsilon_{\mathrm{m}} - \epsilon_{\mathrm{f}})$ is small and should be kept, whereas $3\epsilon_{\mathrm{f}}$ and $(\epsilon_{\mathrm{m}} - \epsilon_{\mathrm{f}})$ can be replaced by $3\epsilon_{\mathrm{s}}$ and $(\epsilon_{\mathrm{m}} - \epsilon_{\mathrm{s}})$. Thus, Eq. (22) can be rewritten as

$$\mathrm{Re}\,[3\epsilon_{\mathrm{s}}(\epsilon_{\mathrm{m}}(\omega) + 2\epsilon_{\mathrm{s}}) - 2(1-f)(\epsilon_{\mathrm{m}}(\omega) - \epsilon_{\mathrm{s}})(\epsilon_{\mathrm{f}} - \epsilon_{\mathrm{s}})] = 0. \tag{23}$$

Let us now introduce the LSPR frequency, $\omega^{\circ}_{\mathrm{LSPR}}$, corresponding to the analyte-free case. This frequency is defined by Eq. (20), i.e.,

$$\mathrm{Re}\,\epsilon_{\mathrm{m}}(\omega^{\circ}_{\mathrm{LSPR}}) + 2\epsilon_{\mathrm{s}} = 0. \tag{24}$$

In the presence of analyte, the LSPR frequency is represented as

$$\omega_{\mathrm{LSPR}} \equiv \omega^{\circ}_{\mathrm{LSPR}} + \Delta\omega_{\mathrm{LSPR}}. \tag{25}$$

This expression can be substituted into the first term in (23), whereas ω in the second term can be replaced by $\omega^{\circ}_{\mathrm{LSPR}}$ (because the latter term is small, and $\Delta\omega_{\mathrm{LSPR}}$ represents there the second-order correction), and then $\epsilon_{\mathrm{m}}(\omega^{\circ}_{\mathrm{LSP}})$ can there be replaced by $-2\epsilon_{\mathrm{s}}$ (as it follows from (24)). This yields

$$\mathrm{Re}\,[\epsilon_{\mathrm{m}}(\omega^{\circ}_{\mathrm{LSPR}}+\Delta\omega_{\mathrm{LSPR}})+2\epsilon_{\mathrm{s}})+2(1-f)(\epsilon_{\mathrm{f}}-\epsilon_{\mathrm{s}})]=0. \tag{26}$$

As already noticed, $\Delta\omega_{\mathrm{LSPR}}$ is small, and accordingly $\epsilon_{\mathrm{m}}(\omega^{\circ}_{\mathrm{LSPR}}+\Delta\omega_{\mathrm{LSPR}})$ can be expanded as

$$\mathrm{Re}\,\epsilon_{\mathrm{m}}(\omega^{\circ}_{\mathrm{LSPR}}+\Delta\omega_{\mathrm{LSPR}})=\mathrm{Re}\,\epsilon_{\mathrm{m}}(\omega^{\circ}_{\mathrm{LSPR}})+\eta\Delta\omega_{\mathrm{LSPR}}, \tag{27}$$

where

$$\eta\equiv\mathrm{Re}\,\frac{\partial\epsilon_{\mathrm{m}}(\omega)}{\partial\omega}\bigg|_{\omega=\omega^{\circ}_{\mathrm{LSP}}}. \tag{28}$$

Substituting (27) into (26) and taking (24) into account, I obtain

$$\Delta\omega_{\mathrm{LSP}}=-2(1-f)(\epsilon_{\mathrm{f}}-\epsilon_{\mathrm{s}})/\eta, \tag{29}$$

or, using (24),

$$\Delta\omega_{\mathrm{LSPR}}=-(2/\eta)(\epsilon_{\mathrm{f}}-\epsilon_{\mathrm{s}})\left(1-\frac{R^3}{(R+d)^3}\right). \tag{30}$$

In terms of the reduction factor employed earlier (in the subsection entitled "Reduction Factors for Specific Systems"), this expression can be rewritten as

$$\Delta\omega_{\mathrm{LSP}}=-(2/\eta)(\epsilon_{\mathrm{f}}-\epsilon_{\mathrm{s}})\left(\frac{3d}{R}\right)\varphi, \tag{31}$$

where

$$\varphi=\frac{R}{3d}\left(1-\frac{R^3}{(R+d)^3}\right). \tag{32}$$

(In this case, $z_{0.5}$ can be identified with $(2^{1/4}-1)R$ or $0.189R$.)

In the context under consideration, the advantage of Eq. (30) (or (31) and (32)) is in its simplicity and transparent derivation without the use of the specific dependence of ϵ_{m} on ω. Regarding this aspect, I recall that often this dependence is represented phenomenologically in the Drude form [40, 43]

$$\epsilon_{\mathrm{m}}=\epsilon_{\infty}-\frac{\omega_{\mathrm{p}}^2}{\omega(\omega+i\gamma)}, \tag{33}$$

so that the LSPR frequency, defined by (20) or (24) in the analyte-free case, is

$$\omega^{\circ}_{\mathrm{LSPR}}=\frac{\omega_{\mathrm{p}}}{(\epsilon_{\infty}+2\epsilon_{\mathrm{s}})^{1/2}}, \tag{34}$$

where ω_{p} is the bulk metal plasmon frequency, and γ ($\ll\omega_{\mathrm{p}}$) is the damping term. Using this expression in (28), one has

$$\eta\simeq 2\omega_{\mathrm{p}}^2/(\omega^{\circ}_{\mathrm{LSPR}})^3. \tag{35}$$

Comparing the expressions obtained here for a spherical plasmonic metal nanoparticle covered by an analyte film ((31) and (32)) with those proposed earlier in the dipole approximation for a film ((3) and (4)), one can draw four conclusions.

(i) The structures of the expressions are similar. In both cases, the response is described by the power-law functions.

(ii) The responses are identical, $\propto d/R_*$ or $\propto d/R$, in the thin-film case.

(iii) The exponents in the power-law term in the reduction factor are different, 5 in (4) and 3 in (32) (see also Fig. 3(b) for a more detailed comparison). The reason of this difference is that the former was proposed for a flat layer, whereas the latter has been derived for a layer covering a sphere. In the former case, an element of volume in the integral expression for the response is just proportional to dz. In the latter case, an element of volume is $4\pi r^2 dr$, where r is the radius. In fact, the results obtained indicate that in applications the intermediate exponent, 4, might be equally applicable or even somewhat better than 5.

(iv) The model under consideration indicates that in the LSPR case one should operate with dielectric permittivities rather than with refractive indexes or, more specifically, with $\epsilon_{\mathrm{f}}-\epsilon_{\mathrm{s}}$ rather than with $n_{\mathrm{f}}-n_{\mathrm{s}}$. This difference is, however, of minor importance, because $\epsilon_{\mathrm{f}}-\epsilon_{\mathrm{s}}$ is anyway proportional to $n_{\mathrm{f}}-n_{\mathrm{s}}$.

Regarding these conclusions, one can notice that the model employed to draw them is based on the Rayleigh approximation and does not take dynamic depolarization into account. To what extent this depolarization should be taken into account depends partly on the properties of plasmonic metal. For Au nanodisks, e.g., the experiments and theoretical analysis based the modified long wave-length approximation indicate that the role of dynamic depolarization is not crucial for diameters up to $\sim$ 150 nm [40]. Roughly, this covers the range of typical sizes of plasmonic nanodisks used in LSPR sensors.

Sensitivity of the LSPR Sensors

The equations derived above can be used to characterize the sensitivity of LSPR sensors with respect to ϵ_{s}, ϵ_{f}, d, or, e.g., the size of sensing plasmonic metal nanoparticles. In general, the sensitivity can be defined in different ways by employing, e.g., the first-order derivatives of λ_{max} with respect to these quantities or the second-order derivatives of λ_{max} with respect of two of them (the latter was proposed in [45]). The use of the first-order derivatives appears to be more natural. For example, one of the physically reasonable dimensionless definitions of the sensitivity with respect to ϵ_{s} and ϵ_{f} is as follows

$$\chi_{\rm i} = \frac{1}{\lambda_{\rm max}}\frac{\partial\lambda_{\rm max}}{\partial\epsilon_{\rm i}} \equiv -\frac{1}{\omega_{\rm LSPR}}\frac{\partial\omega_{\rm LSPR}}{\partial\epsilon_{\rm i}}. \tag{36}$$

where $\epsilon_{\rm i}$ is $\epsilon_{\rm s}$ (i = s) or $\epsilon_{\rm f}$ (i = f). By analogy, the sensitivity with respect to d can be defined as

$$\chi_d = \frac{1}{\lambda_{\rm max}}\frac{\partial\lambda_{\rm max}}{\partial d} \equiv -\frac{1}{\omega_{\rm LSPR}}\frac{\partial\omega_{\rm LSPR}}{\partial d}. \tag{37}$$

In (36) and (37), the derivatives of $\lambda_{\rm max}$ and $\omega_{\rm LSPR}$ with respect to the parameters can be replaced by the corresponding derivatives of $\Delta\lambda_{\rm max}$ and $\Delta\omega_{\rm LSPR}$. In theoretical calculations, one can then use the expressions for $\Delta\lambda_{\rm max}$ and $\Delta\omega_{\rm LSPR}$ presented in the third and fourth subsections above. It can be done, however, with some reservations. In particular, the expressions given in the fourth subsection above contain the sensitivity factor, and its dependence on the parameters is not defined. The expressions derived in the fourth subsection above are physically more complete, but the corresponding model implies that the sensing nanoparticles are spherical and fully surrounded by the analyte film and solution. In real LSPR sensors, the sensing nanoparticles are only partly in close contact with analyte and solution. With these reservations, I use below the expressions $\Delta\omega_{\rm LSPR}$ presented in the fourth subsection above. To take partial contact into account, I multiply the corresponding expressions $\Delta\omega_{\rm LSPR}$ by a factor ξ. Its value is expected to be $\sim 1/3$. In principle, a similar correction can be introduced into Eq. (34) defining $\omega^{\circ}_{\rm LSPR}$, but I do not keep it. In fact, I illustrate how the sensitivity can be calculated. If needed, one can easily perform similar calculations by using the expressions $\Delta\lambda_{\rm max}$ presented in the third subsection above.

With the specification above, the sensitivity of LSPR sensors with respect to $\epsilon_{\rm s}$ can be characterized neglecting a film and substituting (34) into (36),

$$\chi_{\rm s} = \frac{\xi}{\epsilon_\infty + 2\epsilon_{\rm s}}. \tag{38}$$

The sensitivity of LSPR with respect to $\epsilon_{\rm f}$ can be calculated by differentiating (31) and using first (35) for η and then (34),

$$\chi_{\rm f} = \frac{6\xi d}{\eta\omega^{\circ}_{\rm LSPR}R}\varphi = \frac{3\xi(\omega^{\circ}_{\rm LSPR})^2 d}{\omega_{\rm p}^2 R}\varphi = \frac{3\xi d}{(\epsilon_\infty + 2\epsilon_{\rm s})R}\varphi. \tag{39}$$

The sensitivity with respect to d can be calculated by analogy with (39), i.e., by differentiating (30) and using first (35) and then (34),

$$\begin{aligned}\chi_d &= \frac{6\xi(\epsilon_{\rm f}-\epsilon_{\rm s})R^3}{\eta\omega^{\circ}_{\rm LSPR}(R+d)^4} = \frac{3\xi(\epsilon_{\rm f}-\epsilon_{\rm s})(\omega^{\circ}_{\rm LSPR})^2R^3}{\omega_{\rm p}^2(R+d)^4} \\ &= \frac{3\xi(\epsilon_{\rm f}-\epsilon_{\rm s})R^3}{(\epsilon_\infty+2\epsilon_{\rm s})(R+d)^4}.\end{aligned} \tag{40}$$

Conclusions

The indirect LSPR sensors have already been commercialized. To facilitate their use, I have discussed in detail various aspects of the corresponding basic physics. It has been done by employing various models. Although earlier these models were already introduced and discussed in the literature, my presentation contains five novel ingredients:

(i) I have scrutinized the similarities and differences in the formalisms used to interpret SPR and LSPR measurements. In particular, the exponential and power-law attenuation functions have been compared from various perspectives.
(ii) The applicability of the power-law attenuation function has been illustrated by employing the generic model describing spherically shaped sensing plasmonic metal nanoparticles.
(iii) This model has also been used to illustrate the sensitivity of LSPR sensors with respect to various quantities.
(iv) Among more specific results, the available expressions for the signal reduction factor for analyte nanoparticles of various shapes have been collected and complemented by new ones.
(v) In addition, the equation describing the LSPR signal related to analyte attachment to a rough surface has been presented.

Finally, I can repeat that the LSPR and SPR sensors are highly complementary. The former and latter ones are sensitive on the length scales of 10–20 nm and 100–200 nm, respectively. From this perspective, one can mention also QCM-D sensors which are sensitive on the length scale of 250 nm for the first overtone and down to 50 nm for larger overtones [46, 47]. Taken together, these methods operate within the range, from 1 to 500 nm, corresponding to biological soft matter, including proteins, lipids, vesicles, micelles, bicelles, virions, and lipid nanoparticles. Thus, the potential of these methods is far from exhausted, and accordingly the results presented in this work are expected to be useful in the context of various ongoing and following studies.

Acknowledgements I discussed various aspects of the subject under consideration during long-term collaboration with B. Kasemo, I. Zorić, F. Höök, C. Langhammer, N.-J. Cho, and J.A. Jackman. All these contacts are appreciated.

Author Contribution All the work was done by the author.

Funding Open access funding provided by Chalmers University of Technology.

Data Availability The data presented in this study are available in the article.

Code Availability Not applicable.

Declarations

Ethical Approval Not applicable.

Conflict of Interest The author declares no competing interests.

References

1. Mulvaney P, Buriak JM, Chen X, Hu T (2022) Nanoscience and entrepreneurship. ACS Nano 16:6943–6944
2. Bayda S, Adeel M, Tuccinardi T, Cordani M, Rizzolio F (2020) The history of nanoscience and nanotechnology: from chemical-physical applications to nanomedicine. Molecules 25:112
3. Stockman MI et al (2018) Roadmap on plasmonics. J Optics 20:043001
4. Jiang NN, Zhuo XL, Wang JF (2018) Active plasmonics: principles, structures, and applications. Chem Rev 118:3054–3099
5. Linic S, Chavez S, Elias R (2021) Flow and extraction of energy and charge carriers in hybrid plasmonic nanostructures. Nature Mater 20:916–924
6. Larsson EM, Syrenova S, Langhammer C (2012) Nanoplasmonic sensing for nanomaterials science. Nanophotonics 1:249–266
7. Nugroho FAA et al (2019) Metal-polymer hybrid nanomaterials for plasmonic ultrafast hydrogen detection. Nature Mater 18:489–495
8. Mamatkulov M, Zhdanov VP (2021) Partial or complete suppression of hysteresis in hydride formation in binary alloys of Pd with other metals. J Alloys Comp 885:160956
9. Jackman JA, Ferhan AR, Cho N-J (2017) Nanoplasmonic sensors for biointerfacial science. Chem Soc Rev 46:3615–3660
10. Mauriz E, Dey P, Lechuga LM (2019) Advances in nanoplasmonic biosensors for clinical applications. Analyst 144:7105–7129
11. dos Santos PSS, de Almeida MMMJ, Pastoriza-Santos I, Coelho LCC (2021) Advances in plasmonic sensing at the NIR - a review. Sensors 21:2111
12. Kim DM, Park JS, Jung S-W, Yeom J, Yoo SM (2021) Biosensing applications using nanostructure-based localized surface plasmon resonance sensors. Sensors 21:3191
13. Xu T, Geng Z (2021) Strategies to improve performances of LSPR biosensing: structure, materials, and interface modification. Biosens Bioelectr 174:112850
14. Nocerino V, Miranda B, Tramontano C, Chianese G, Dardano P, Rea I, De Stefano L (2022) Plasmonic nanosensors: design, fabrication, and applications in biomedicine. Chemosensors 10:150
15. Jackman JA et al (2017) Indirect nanoplasmonic sensing platform for monitoring temperature-dependent protein adsorption. Anal Chem 89:12976–12983
16. Tan JYB et al (2020) Unraveling how ethanol-induced conformational changes affect BSA protein adsorption onto silica surfaces. Langmuir 36:9215–9224
17. Yoon BK et al (2021) Solvent-induced conformational tuning of lysozyme protein adlayers on silica surfaces: a QCM-D and LSPR study. Int J Biol Macromol 182:1906–1914
18. Jackman JA, Zhdanov VP, Cho N-J (2014) Nanoplasmonic biosensing for soft matter adsorption: kinetics of lipid vesicle attachment and shape deformation. Langmuir 30:9494–9503
19. Oh E et al (2015) Contribution of temperature to deformation of adsorbed vesicles studied by nanoplasmonic biosensing. Langmuir 31:771–781
20. Jackman JA et al (2016) Nanoplasmonic ruler to measure lipid vesicle deformation. Chem Commun 52:76–79
21. Jackman JA et al (2017) Quantitative profiling of nanoscale liposome deformation by a localized surface plasmon resonance sensor. Anal Chem 89:1102–1109
22. Ferhan AR et al (2018) Nanoplasmonic sensing architectures for decoding membrane curvature-dependent biomacromolecular interactions. Anal Chem 90:7458–7466
23. Asai N, Matsumoto N, Yamashita I, Shimizu T, Shingubara S, Ito T (2021) Detailed analysis of liposome adsorption and its rupture on the liquid-solid interface monitored by LSPR and QCM-D integrated sensor. Sens Bio-Sens Res 32:100415
24. Park H et al (2021) Unraveling how multivalency triggers shape deformation of sub-100 nm lipid vesicles. J Phys Chem Lett 12:6722–6729
25. Park H et al (2022) Multivalency-induced shape deformation of nanoscale lipid vesicles: size-dependent membrane bending effects J Phys Chem Lett 13:1480–1488
26. Park H et al (2022) Unraveling how cholesterol affects multivalency-induced membrane deformation of sub-100 nm lipid vesicles. Langmuir 38:15950–15959
27. Nugroho FAA et al (2022) Time-resolved thickness and shape-change quantification using a dual-band nanoplasmonic ruler with sub-nanometer resolution. ACS Nano 16:15814–15826
28. Yoon BK, Park H, Zhdanov VP, Jackman JA, Cho N-J (2021) Real-time nanoplasmonic sensing of three-dimensional morphological changes in a supported lipid bilayer and antimicrobial testing applications. Biosens Bioelectron 174:112768
29. Liedberg B, Nylander C, Lundström I (1995) Biosensing with surface plasmon resonance - how it all started. Biosens Bioelectron 10:i–ix
30. Homola J (2008) Surface plasmon resonance sensors for detection of chemical and biological species. Chem Rev 108:462–493
31. Nguyen HH, Park J, Kang S, Kim M (2015) Surface plasmon resonance: a versatile technique for biosensor applications. Sensors 15:10481–10510
32. Larsson EM, Edvardsson MEM, Langhammer C, Zorić I, Kasemo B (2009) A combined nanoplasmonic and electrodeless quartz crystal microbalance setup. Rev Sci Inst 80:125105
33. Jung LS, Campbell CT, Chinowsky TM, Mar MN, Yee SS (1998) Quantitative interpretation of the response of surface plasmon resonance sensors to adsorbed films. Langmuir 14:5636–5648
34. Rupert DLM et al (2016) Dual-wavelength surface plasmon resonance for determining the size and concentration of sub-populations of extracellular vesicles. Anal Chem 88:9980–9988
35. Rechendorff K, Hovgaard MB, Foss M, Zhdanov VP, Besenbacher F (2006) Enhancement of protein adsorption induced by surface roughness. Langmuir 22:10885–10888
36. Olsson T, Zhdanov VP, Höök F (2015) Total internal reflection fluorescence microscopy for determination of size of individual immobilized vesicles: theory and experiment. J Appl Phys 118:064702
37. Czajkowski KM, Antosiewicz TJ (2020) Effective dipolar polarizability of amorphous arrays of size-dispersed nanoparticles. Optics Lett 45:3220–3223
38. Purcell TAR, Yochelis S, Paltiel Y, Seideman T (2018) Determining the molecular dipole orientation on nanoplasmonic structures. J Phys Chem C 122:16901–16908
39. Xiang H, Zu J, Jiang H, Xu L, Lu G, Zhang X (2022) Understanding quantum plasmonic enhancement in nanorod dimers

from time-dependent orbital-free density functional theory. J Phys Chem C 126:5046–5054
40. Zorić I, Zäch M, Kasemo B, Langhammer C (2011) Gold, platinum, and aluminum nanodisk plasmons: material independence, subradiance, and damping mechanisms. ACS Nano 5:2535–2546
41. Bohren CF, Huffman DR (2004) Absorption and scattering of light by small particles. Wiley, Weinheim
42. Kulkarni V, Prodan E, Nordlander P (2013) Quantum plasmonics: optical properties of a nanomatryushka. Nano Lett 13:5873–5879
43. Mulvaney P (1996) Surface plasmon spectroscopy of nanosized metal particles. Langmuir 12:788–800
44. Ma Y-W, Zhang J, Zhang L-H, Jian S-F (2011) Theoretical analysis the optical properties of multi-coupled silver nanoshell particles. Plasmonics 6:705–713
45. Li J et al (2015) Revisiting the surface sensitivity of nanoplasmonic biosensors. ACS Photonics 2:425–431
46. Armanious A, Agnarsson B, Lundgren A, Zhdanov VP, Höök F (2021) Determination of nanosized adsorbate mass in solution using mechanical resonators: elimination of the so far inseparable liquid contribution. J Phys Chem C 125:22733–22746
47. Ma GJ, Zhdanov VP, Park S, Sut TN, Cho N-J (2021) Mechanistic aspects of the evolution of 3D cholesterol crystallites in a supported lipid membrane via a quartz crystal microbalance with dissipation monitoring. Langmuir 37:4562–4570